

Characterization of liquid and gaseous micro- and nanojets using microcantilever sensors

Jungchul Lee^a, Kianoush Naeli^b, Hanif Hunter^a, John Berg^a, Tanya Wright^a,
Christophe Courcimault^b, Nisarga Naik^b, Mark Allen^b, Oliver Brand^b,
Ari Glezer^a, William P. King^{a,*}

^a Woodruff School of Mechanical Engineering, Georgia Institute of Technology, Atlanta, GA 30332-0405, United States

^b School of Electrical and Computer Engineering, Georgia Institute of Technology, Atlanta, GA 30332-0250, United States

Received 28 February 2006; received in revised form 4 May 2006; accepted 5 May 2006

Available online 30 June 2006

Abstract

This paper reports the development of microelectromechanical metrology tools to characterize liquid and gaseous jets generated from micro-fabricated nozzles with diameters ranging from 1 to 12 μm . Microcantilever sensors with either piezoresistive elements or integrated heating elements have been fabricated and applied to measure thrusts, velocities, and heat transfer characteristics of micro/nanojets. Piezoresistive cantilever measurements showed that liquid butane microjets from a 6 μm diameter nozzle achieved velocities 40–60 m/s for driving pressures 0.6–1.4 MPa. Jet velocities estimated from cantilever measurements agreed well with shadowgraphy results within 12.5% without any correction factor. A microcantilever with integrated heating elements measured cooling capacities of liquid butane microjets on the order of 10^{-5} W/K.

© 2006 Published by Elsevier B.V.

Keywords: MEMS; Microcantilever; Microjets; Nanojets; Hot-wire; Thrust; Shadowgraphy

1. Introduction

Micro/nanoscale jets have potential applications in drug delivery [1], microsurgery [2], inkjet printing [3], microelectronics cooling [4,5], and precision manufacturing [6]. While $O(100\text{--}1000 \mu\text{m})$ -scale high speed gaseous jets have been investigated as potential actuators for flow control applications, little work has been reported on free liquid and gaseous jets having characteristic scales that extend below 10 μm the jet diameter becomes comparable to or even smaller than the wavelength of the light source employed, optical metrology such as particle image velocimetry (PIV) and laser Doppler velocimetry may not be viable. Hot-wire anemometry (HWA) has been miniaturized using microfabrication techniques [7] but its size is still comparable to or larger than the nozzle diameters, such that hot-wire sensors could not be fully submerged into micro/nanoscale flows. Moreover, the hot-wire is generally too fragile to be inter-

faced with liquid jet environment. Flow visualization techniques such as Schlieren photography, interferometry, and shadowgraphy are also challenging even for the liquid jets that have a distinctive refractive index compared to the ambient.

Microfabricated cantilevers have become perhaps the most widely used transducer for sensing and actuating at the nanometer scale [8] with the major application being atomic force microscopy (AFM). In AFM operation, a force can bend the cantilever and the amount of deflection is recorded using various mechanisms such as optical sensing [9,10], piezoresistive sensing [11,12], capacitive sensing [13], and thermal sensing [14,15]. Besides AFM application, microfabricated cantilevers have been employed for acceleration sensing [16], bio/chemical detection [17–20], radio frequency microelectromechanical systems (MEMS) switches [21], local control of chemical vapor deposition processes [22], and nanoscale deposition of solid materials [23,24].

Recently, microcantilevers also have been used as metrology tools to measure fluid properties and investigate flow characteristics. Micromachined silicon cantilever beams have been applied in liquid flow volume sensing [25,26] and highly sensitive

* Corresponding author. Tel.: +1 404 385 4224; fax: +1 404 894 8496.

E-mail address: william.king@me.gatech.edu (W.P. King).

piezoresistive cantilevers have been introduced for measuring air flow velocity in a small pipe [27]. Microcantilevers immersed in viscous fluid have been characterized [28] and applied to measure viscous drag [29]. AFM cantilever based anemometers have been designed to measure gas and liquid flows with high spatial and temporal resolution and demonstrated turbulent flow measurements in both air and water [30]. Due to their high deflection sensitivity and small minimum detectable deflection in the sub-nanometer regime, microcantilevers are promising candidates for micro/nanojets flow characterization.

Among microcantilever sensing mechanisms, piezoresistive and thermal sensing are best suited for liquid and gaseous jets environment. With the liquid jet impingement, optical sensing using a laser and position sensitive diode could generate spurious signals due to the refraction in the liquid around the cantilever. Capacitive sensing usually requires electrode structures that could block the jet flow and limit cantilever deflection. Free standing structures are preferred for micro/nanojets metrology since they can be fully exposed to the jet environment. Piezoresistive sensing is well suited for deflection, thrust, and velocity measurement for both liquid and gaseous micro/nanojets. Since a commercial piezoresistive cantilever

was readily available, it was introduced to verify the working concepts. After that, customized piezoresistive cantilevers were fabricated considering problems associated with the commercial cantilevers.

For heat flux measurements of micro/nanojets, another type of cantilever which has an integrated heating element (heated cantilever) was introduced. The heated cantilevers were originally developed for data storage [31,32], but have recently been redesigned and fabricated at Georgia Tech to extend their functionality. By mimicking HWA, the heated cantilever can interrogate the cooling capacity of micro/nanojets by monitoring heat transfer between the integrated heating element and micro/nanojets environment.

Based on previously reported work [33], this paper presents novel metrology applications of microfabricated cantilevers to investigate micro/nanojets flow. The jets were generated from micromachined silicon nozzles defined in the chip plane, connected to a small-scale pressurized reservoir [34]. Liquid butane and gaseous nitrogen jets ejected from 1 to 12 μm diameter nozzles have been characterized with the microcantilever sensors. Piezoresistive cantilevers were used to extract jet thrust and velocity from the measured beam deflection and heated can-

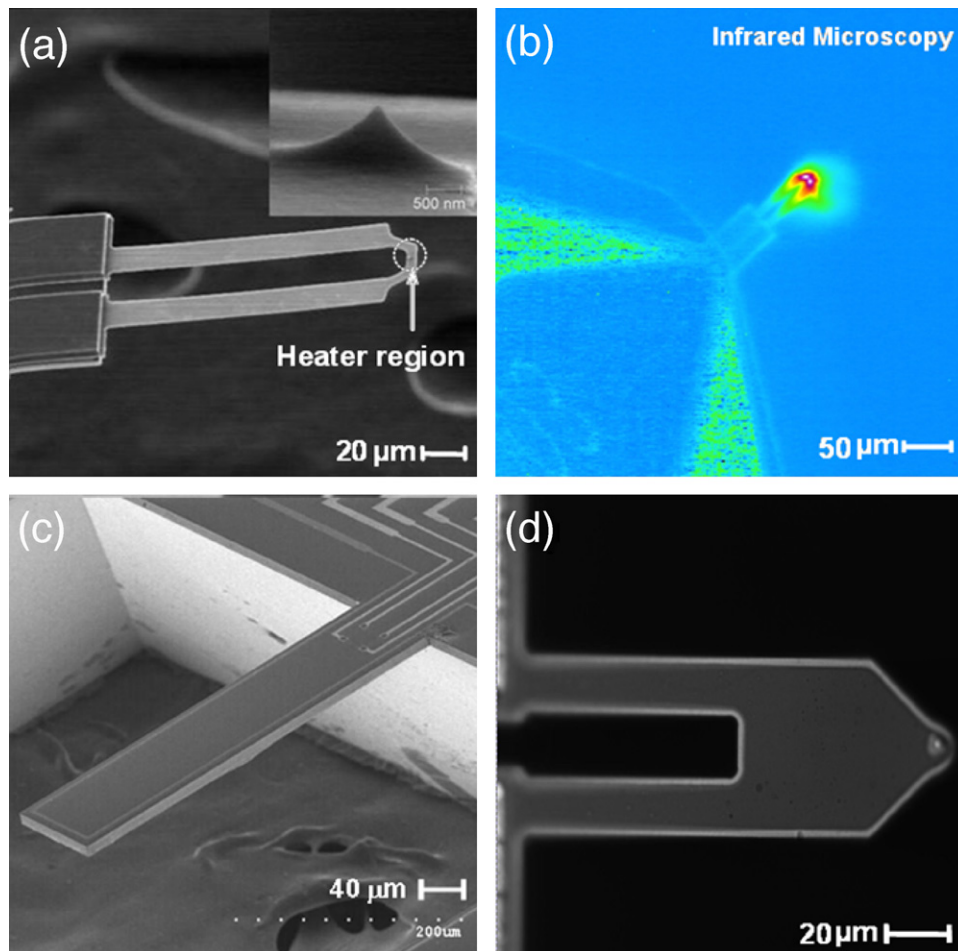


Fig. 1. (a) SEM micrograph of a fabricated heated cantilever; (b) IR micrograph of the fabricated heated cantilever with electrical heating; (c) SEM micrograph of a fabricated piezoresistive cantilever; (d) optical micrograph of a commercial piezoresistive cantilever.

tilers were used to estimate either the heat transfer coefficient or cooling capacity of micro/nanojets.

2. Experiments

The experimental setup consisted of a high pressure fluidic system including microfabricated nozzles, optical diagnostic tools, high resolution positioning systems, and microcantilever sensors. Fig. 1(a and b) shows scanning electron microscope (SEM) and infrared (IR) microscope images of a fabricated microcantilever heater, respectively. Fig. 1(c and d) shows a SEM image of a fabricated piezoresistive cantilever and an optical micrograph of a commercially available piezoresistive cantilever, respectively.

The heated AFM cantilevers were made using a standard silicon-on-insulator (SOI) process generally following a documented fabrication process [31] but modified to suit our fabrication facility [35] and briefly summarized as follows. The fabrication process started with a SOI wafer of orientation (100), n-type doping at $2 \times 10^{14} \text{ cm}^{-3}$ having a resistivity of approximately $4 \Omega \text{ cm}$. The cantilever tip was formed using an oxidation sharpening process [36] and had a radius of curvature near 20 nm. The cantilever was made electrically active through two phosphorous doping steps: first, the two parallel cantilever legs were doped to $1 \times 10^{20} \text{ cm}^{-3}$ and the heater region near the free end of the cantilever was doped to $1 \times 10^{17} \text{ cm}^{-3}$. After metallization and lift-off to define aluminum contacts, the backside of the handle wafer was etched by reactive ion etch (RIE) until the buried oxide layer was exposed. The cantilevers were finally released by 15 s dip in 49% hydrofluoric acid.

Besides using commercially available piezoresistive cantilevers, silicon cantilevers with an embedded full piezoresistive Wheatstone bridge have been fabricated to minimize temperature effects due to jet cooling while monitoring jet thrust. Assuming that all four resistors on the cantilever see approximately the same temperature, temperature changes will not cause a bridge output signal. The particular cantilever shown in Fig. 1(c) has a length and width of 400 and 80 μm , respectively, and is comprised of a 6 μm thick n-type epitaxial layer, covered by a 1.0 μm PECVD silicon dioxide film. The embedded piezoresistive Wheatstone bridge uses a picture-frame layout with diffused p-type resistors having a final sheet resistance of 65 Ω/\square . The electrical interconnects are formed by 200 nm thick aluminum lines. A metal line running along the perimeter of the cantilever can be used for magnetic excitation of the cantilever at its resonance frequency at 54 kHz, allowing us to measure the mass deposition by the microjet. The cantilevers are released by a combination of anisotropic wet etching from the back of the wafer using a 6M KOH solution and an electrochemical etch-stop technique and RIE from the front of the wafer to define the final lateral dimensions.

Fig. 2 shows the experimental setup that accommodates the two different types of microcantilever sensors. Both microcantilever and microfabricated nozzle are controlled by independent three-axis motorized transverse stages with 50 nm resolution. The flow field is illuminated using a double-pulse ND:YAG laser (532 nm) where the pulse duration is on the order of 5 ns.

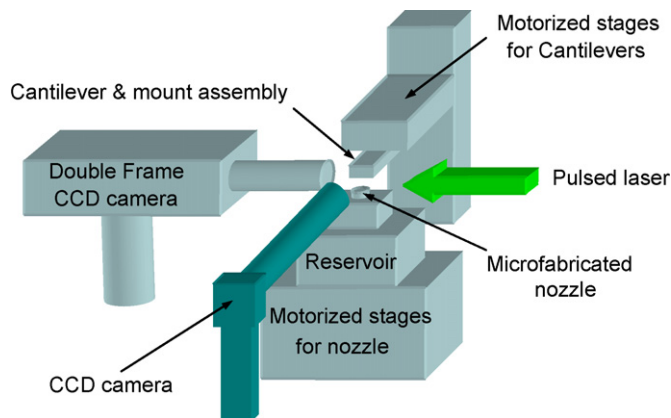


Fig. 2. Experimental setup which enables to switch two different types of microcantilever sensors. Double frame CCD camera with pulsed laser is used for shadowgraphy and normal CCD camera with co-axial illumination is configured for monitoring cantilever motion and coarse alignment. Both microcantilever sensor and microfabricated nozzle are mounted on independent 3-axis motorized stages.

Instantaneous images of the flow are captured using a PIV charge coupled device (CCD) camera having 1008×1018 pixels equipped with a high-magnification microscope lens. The lens system consists of a $50\times$ infinity corrected microscope objective lens coupled with a 6.5:1 zoom lens having 0.7–4.5 zoom ratio for a total maximum magnification of $228\times$. The smallest achievable field of view measures 28 μm on the side. For coarse alignment and quick inspection, another CCD camera in conjunction with a 12:1 zoom lens and a $5\times$ microscope objective lens is configured.

Measurements were made on jets of liquid butane and gaseous nitrogen. Liquid butane has a surface tension of 0.0123 N/m and a vapor pressure of 0.22 MPa at standard temperature and pressure. Fig. 3 shows the constructed fluidic system which can generate high-speed sub-micrometer-scale jets. In this system, nitrogen was used for pressurizing. The maximum operating pressure of the present system was 34.5 MPa. The system was vacuumed to remove air as far as possible and then the

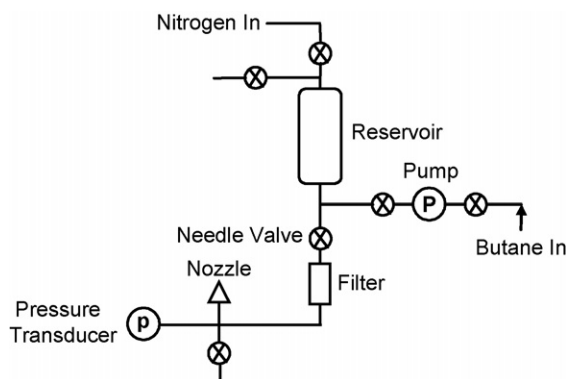


Fig. 3. Fluidic system diagram. The maximum operating pressure of the present system is 34.5 MPa. Before the system is filled with liquid butane, it is first pressurized slightly above its vapor pressure using nitrogen, and then butane is pumped into the reservoir to the desired level. The system is then pressurized again to the desired driving pressure using nitrogen. Both liquid and gaseous micro/nanojets can be driven with this fluidic system.

liquid butane was pumped into the reservoir to the desired level. The system was then pressurized to the desired driving pressure using nitrogen. The microfabricated nozzle was directly connected to the reservoir and designed to minimize volume and the possibility of nitrogen pockets. With the needle valve to the liquid butane supply closed, gaseous nitrogen jets could be driven.

Once the position of the nozzle and reservoir assembly was fixed, the piezoresistive cantilevers were brought close to the jet and scanned over the entire effective flow field. The pre-calibrated commercial piezoresistive cantilever with its single piezoresistor was embedded in an off-chip Wheatstone bridge, whose output signal was amplified by a differential amplifier. The cantilevers with embedded piezoresistive Wheatstone bridge were directly interfaced with the measurement equipment. The heated cantilever was stationary such that the heating element near its tip could be fully exposed to the jet environment during jet impingement. Since the resistance change of the heated cantilever was much larger than that of the piezoresistive cantilever, measurements were done with a voltage divider having one off-chip resistor connected in series to the cantilever heater. All cantilever types were powered by a Keithley SourceMeter 2400 and monitored by an Agilent 34401A multimeter. Both liquid and gaseous jets were tested using two different types of microcantilevers.

3. Cantilever calibration

The experimental procedure began with calibration of the microcantilever sensors. The temperature of the liquid butane jet is well below room temperature while the temperature of the gaseous nitrogen jet is close to room temperature. Since piezoresistive cantilevers with a single piezoresistor are sensitive to deflection and temperature, they must be calibrated independently for both. A calibration setup was constructed using a precise motorized micro-transverse stage and an optical microscope. Fig. 4 shows the calibration results of a

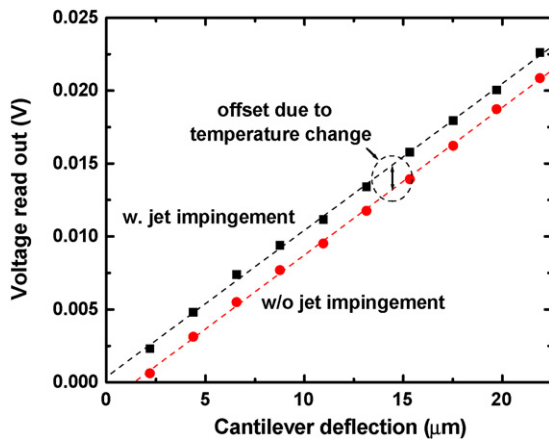


Fig. 4. Voltage read out from a Wheatstone bridge as a function of deflection of the commercial piezoresistive cantilever with 2 V bias voltage. Both calibrations with and without jet impingement show the same deflection sensitivity. The offset due to environmental temperature change should be considered to get actual cantilever deflection.

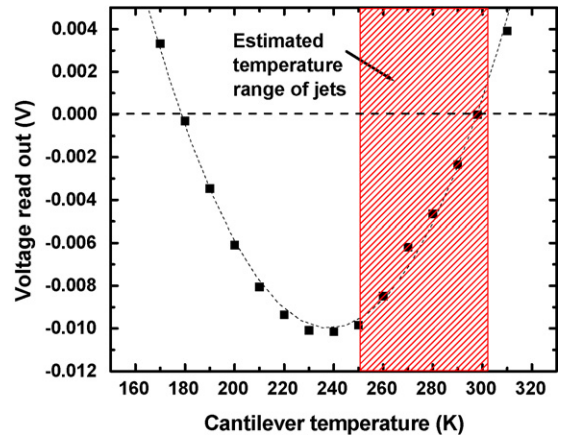


Fig. 5. Temperature calibration results of a commercial piezoresistive cantilever. Wheatstone bridge outputs were measured at different cantilever temperatures in the cryostat. The sensor read out changes in a parabolic fashion with the sensor temperature under the assumption of thermal equilibrium between the piezoresistive cantilever and the mounting stage in the cryostat.

commercial piezoresistive cantilever embedded in an off-chip Wheatstone bridge with applied deflection. The voltage from the Wheatstone bridge increases linearly with cantilever deflection. The calibration was repeated during liquid jet impingement. The deflection sensitivity with jet impingement was identical to that without jet impingement such that each output due to mechanical deflection and temperature change could be added together.

Silicon piezoresistors exhibit a strong temperature coefficient of resistance (TCR), and any cantilever with a single piezoresistor must be temperature compensated to obtain the actual cantilever deflection. To this end, the commercial piezoresistive cantilever was placed in a cryostat to check the temperature dependence of the cantilever resistance as shown in Fig. 5. The sensor read out changes in a parabolic fashion with the sensor temperature under the assumption of thermal equilibrium between the cantilever and the mounting stage in the cryostat. The piezoresistive cantilever signal, V , is approximated by

$$V = a\delta + b(T - T_c)^2 + c \tag{1}$$

where δ is cantilever deflection, T the effective temperature of surroundings, T_c the critical temperature where $\partial V/\partial T=0$, a the deflection sensitivity, b the temperature sensitivity, and c is the maximum temperature offset at the critical temperature.

In contrast to the piezoresistive cantilever, the heated cantilever is barely sensitive to the applied deflection, and only a temperature calibration with electrical power excitation is required. Since the heated cantilever consists of highly doped conductive legs and a low doped resistive heater, there is well known effect called “thermal runaway” where the cantilever TCR changes from positive to negative [37]. The resistance of the heated cantilever was calibrated using a Quantum Focus Instruments InfraScope II IR microscope with electrical heating at relatively low temperature where the cantilever shows positive TCR and results are shown in Fig. 6.

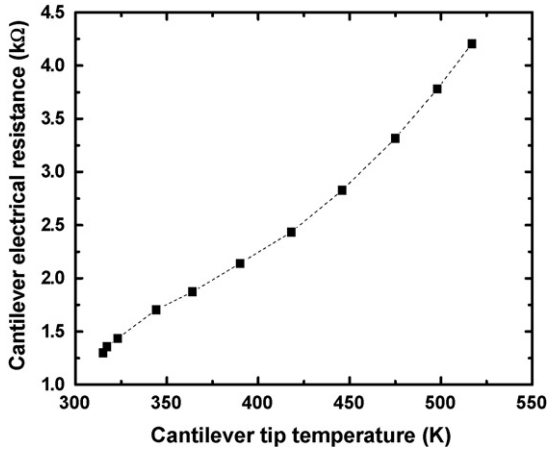


Fig. 6. Measured electrical resistance of a heated AFM cantilever as a function of cantilever tip temperature calibrated using an infrared microscope. The resistance of the heated cantilever was calibrated using an IR microscope at relatively low temperature where the heated cantilever has positive TCR.

4. Results and discussion

4.1. Piezoresistive cantilever sensor

Piezoresistive cantilevers were employed first to estimate thrusts and velocities of the micro/nanojets. The piezoresistive cantilever was scanned over the effective flow field of both liquid and gaseous micro/nanojets. During scanning, the sensor outputs were recorded and processed to extract the actual deflection of the cantilever using the aforementioned calibration results. Then, cantilever deflections were used to extract jet thrusts and velocities.

Fig. 7 shows the commercial piezoresistive cantilever impinged by a liquid butane jet from a 12 μm diameter nozzle. The cantilever shows a significant deflection of about 20 μm when the liquid jet impinges on its bottom side and the liquid

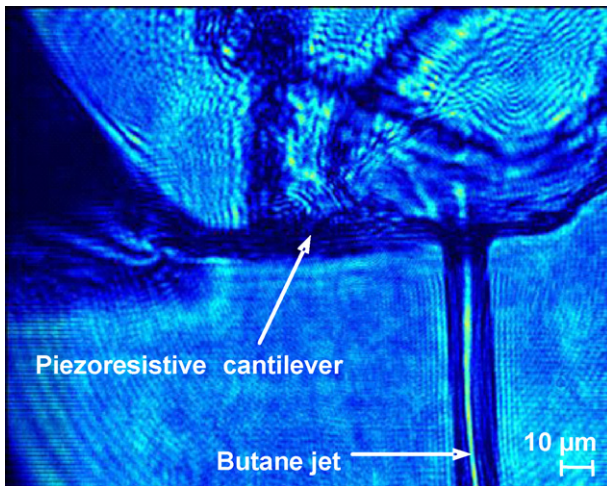


Fig. 7. Piezoresistive cantilever deflects when the liquid butane jets impinge on the bottom surface of the cantilever. Small portion of the butane jets still have vertical direction velocity components after impinging on the piezoresistive cantilever. Momentum of liquid jets is not fully transferred to the cantilever when the nozzle diameter is comparable to the cantilever width.

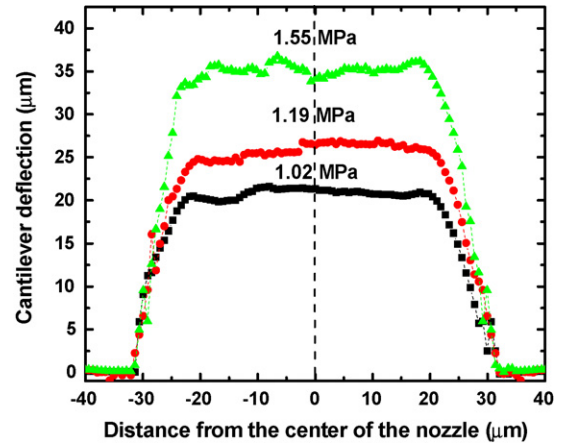


Fig. 8. Deflection of the commercial piezoresistive cantilever as the cantilever is traversed through liquid butane jets where butane microjets are generated from a 6 μm microfabricated nozzle with 130 μm separation between the cantilever and the nozzle. Each deflection curve has a plateau which indicates that the cantilever deflection is nearly constant once the jets are blocked completely by the cantilever and there is negligible torsional motion.

butane jet still has a small portion of vertical direction velocity component after impinging the cantilever. We conclude that the vertical momentum of the liquid jet is not fully transferred to the cantilever.

Fig. 8 shows the measured cantilever deflection as the cantilever is traversed through liquid butane jets generated from a 6 μm microfabricated nozzle with 130 μm separation between the cantilever and the nozzle. Each deflection curve has a plateau which indicates that the cantilever deflection is nearly constant once the liquid butane jet is blocked completely by the cantilever and there is negligible torsional motion.

When the liquid butane jet is aligned to the center of the cantilever in the scanning direction, the jet thrust, F , can be obtained by

$$F = \frac{2L^3}{d^2(3L - d)}k\delta \quad (2)$$

with the assumption that the piezoresistive cantilever has a uniform rectangular cross-section from its free end to clamped base and experiences pure bending. L is the cantilever length, d the distance from the clamped base to the center of the jet, and k is the spring constant [38]. The distance d was measured with a PIV CCD camera and the spring constant ($k = 1.4 \text{ N/m}$) of the commercial piezoresistive cantilever was obtained using an AFM system before jet testing. The jet velocity, v , could be estimated by

$$v = \sqrt{\frac{F}{C\rho A_{\text{jet}}}} \quad (3)$$

where C is the momentum transfer correction factor, ρ the density of the fluid, and A_{jet} is the cross-sectional area of the jet [39].

Three assumptions are made to estimate the jet velocity. First, the cross-section of the liquid jet is a perfect circle with a diameter measured using a PIV CCD camera. Second, the density of

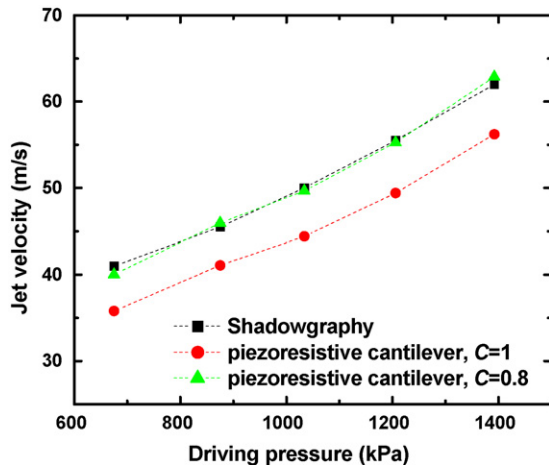


Fig. 9. Measured jet velocities as a function of driving pressure extracted from the piezoresistive cantilever measurements and shadowgraphy. Since jet momentum is partially transferred to the cantilever when the nozzle diameter is comparable to the size of the cantilever, a momentum transfer correction factor, C needs to be introduced for better velocity estimation. When $C = 1$, the piezoresistive cantilever measurements have no more than 12.5% error. The velocity data obtained from the piezoresistive cantilever show best agreement with the measured velocity using the shadowgraphy when $C = 0.8$.

the liquid jet does not change much with driving pressure after the jet is ejected from the nozzle. The third assumption is that a momentum transfer correction factor should be introduced for better estimation since momentum of the liquid jet is not completely transferred to the cantilever when the nozzle diameter is comparable to the cantilever physical dimension. Eq. (3) calculates jet velocities at different driving pressures with and without a reasonable correction factor and Fig. 9 compares the results with jet velocities obtained using laser shadowgraphy. When $C = 1$, the piezoresistive cantilever measurements have no more than 12.5% error. The velocity data obtained from the piezoresistive cantilever measurements show best agreement with the shadowgraphy results when $C = 0.8$ meaning 80% of the jet momentum is actually transferred to the cantilever. The momentum transfer correction factor will approach unity as the nozzle size gets smaller such that more accurate velocity measurement can be made with nozzles having sub-micrometer diameter.

The cantilevers with embedded piezoresistive Wheatstone bridge were used to characterize liquid butane jets ejected from a $10\ \mu\text{m}$ nozzle with square cross-section. Fig. 10 shows the extracted deflection based on the output signal of the Wheatstone bridge biased with 1 V as the cantilever is traversed across the jet. The deflection sensitivity of the cantilever is $1.01\ \text{mV}/\mu\text{m}$ for a bridge bias of 1 V and was measured by deflecting the cantilever tip with a probe tip mounted on a micropositioning stage, while monitoring the deflection through an optical microscope. The jet impinges onto the cantilever at a distance of approximately $50\ \mu\text{m}$ from the tip, the distance from orifice to cantilever was $480\ \mu\text{m}$ and the scanning speed was $0.7\ \mu\text{m}/\text{s}$. The recorded piezoresistive signal is the result of a convolution of the cross-section of the jet (with a diameter of about $15\ \mu\text{m}$ at $480\ \mu\text{m}$ distance from the orifice) and the width of the cantilever. As a result, the cantilever is deflected for a scanning distance larger than the actual cantilever width of $80\ \mu\text{m}$. As we scan the can-

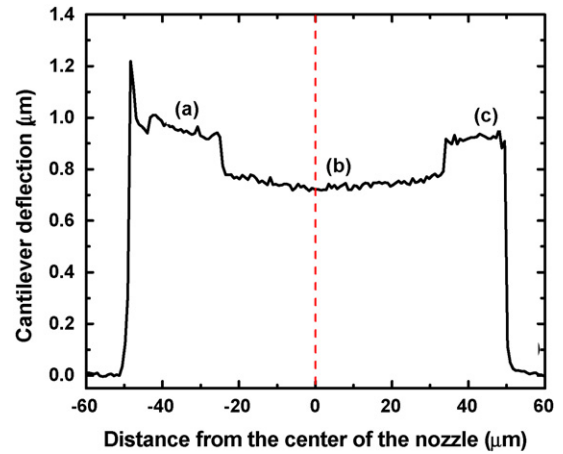


Fig. 10. Deflection of the piezoresistive cantilever with embedded Wheatstone bridge while scanning a liquid butane jet ejected from a $10\ \mu\text{m} \times 10\ \mu\text{m}$ square nozzle at a pressure of 3.8 MPa across the cantilever with a speed of $0.7\ \mu\text{m}/\text{s}$; the jet impinges on the cantilever $50\ \mu\text{m}$ from its free end and the distance between nozzle and cantilever is approximately $480\ \mu\text{m}$; the cantilever has a deflection sensitivity of $1.01\ \text{mV}/\mu\text{m}$ at 1 V bias.

tiler across the jet, we can identify three distinct regimes. A first peak in the piezoresistive signal usually appears when the jet first impinges on the cantilever. After this initial peak, the deflection first stabilizes until it suddenly drops by approximately $0.2\ \mu\text{m}$. The observed pattern is symmetric and we see a sudden increase in deflection by $0.2\ \mu\text{m}$ as we continue to scan across the beam. Just before the jet stops impinging on the surface, another, usually less pronounced, peak is observed. The jet coming from a $10\ \mu\text{m}$ nozzle deposits significant liquid butane in form of liquid bubbles on the cantilever. After starting to impinge on the cantilever, butane bubbles initially form on both the upstream and downstream sides of the cantilever (region (a) in Fig. 10). Once the jet is completely blocked by the cantilever, only its upstream side is wetted by the bubbles and the deflection reduces by approximately $0.2\ \mu\text{m}$ (region (b)). Finally, while leaving the cantilever, bubbles again form on both sides (region (c)). During impingement, butane bubbles frequently form and evaporate, resulting in small transient peaks in the output signal. Using the simulated spring constant ($k = 14.5\ \text{N}/\text{m}$) of the fabricated cantilever, a thrust and jet velocity of approximately $12\ \mu\text{N}$ and $10\ \text{m}/\text{s}$ can be estimated for the liquid butane microjet ejected from the $10\ \mu\text{m}$ nozzle ($P = 3.8\ \text{MPa}$) at $480\ \mu\text{m}$ distance from the orifice.

Gaseous micro/nanojets were also tested using the same fluidic system with the needle valve for liquid butane supply closed. Fig. 11 shows the measured cantilever deflection as the commercial piezoresistive cantilever is traversed through gaseous nitrogen jets generated from a $1\ \mu\text{m}$ microfabricated nozzle with $27\ \mu\text{m}$ separation distance between the cantilever and the nozzle. The driving pressure varies from 6.8 to 10.6 MPa. In contrast to the liquid jet, the gaseous jet shows almost symmetric deflection curves having a maximum deflection when the cantilever is aligned to the center of the nozzle. As an example, Fig. 11(b) shows a Gaussian-like deflection curve when the driving pressure is 9.65 MPa [see cross-section AA' in Fig. 11(a)].

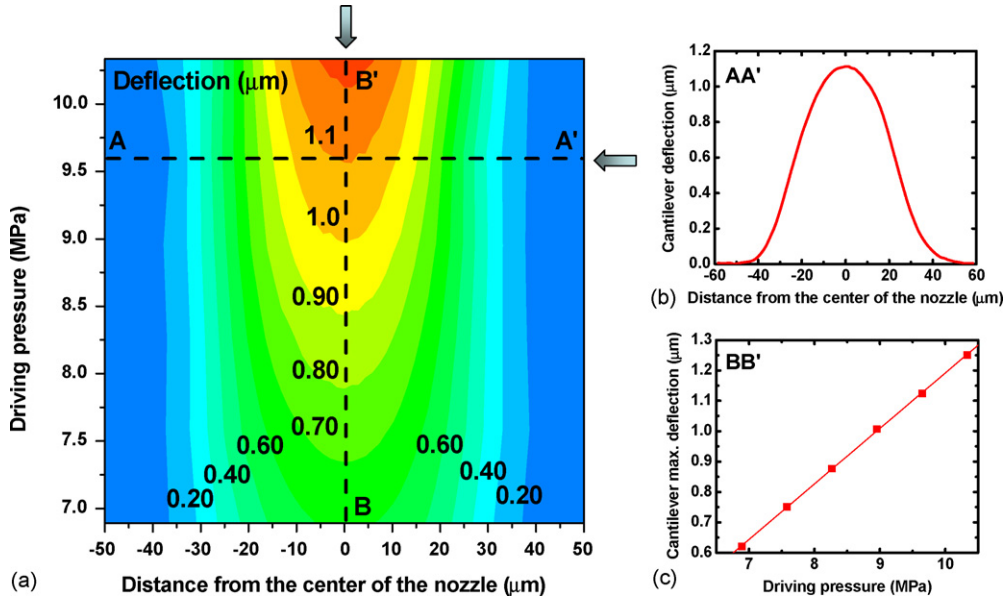


Fig. 11. (a) Contour plot of deflection of the piezoresistive cantilever as the cantilever is traversed through gaseous nitrogen jets. (b) A Gaussian-like deflection curve when the driving pressure is 9.65 MPa. (c) Linear relationship between cantilever maximum deflection and driving pressure. Gaseous nitrogen jets are generated from a 1 μm diameter nozzle with 27 μm separation between the cantilever and the nozzle.

Fig. 11 also shows that the effective flow field of the gaseous nitrogen jet does not change within the tested pressure range. The effective flow field of gaseous nitrogen jet was much wider than that of liquid butane jet even though a much smaller diam-

eter nozzle was configured. It can be inferred that the gaseous jet sprays out while the cross-section of the liquid jet remains uniform as shown in Fig. 12 even though the gaseous jet cannot be visualized at the moment. With the cantilever physical

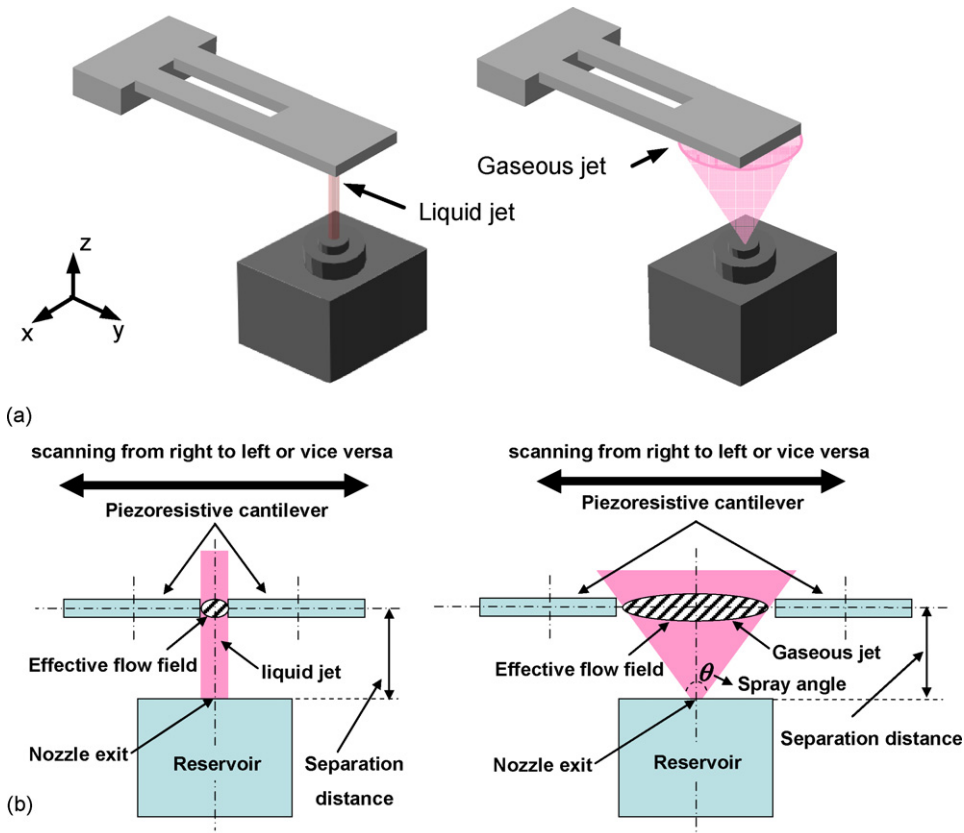


Fig. 12. (a) Configuration of nozzle and cantilever for liquid and gaseous jets. In contrast to liquid jets, gaseous jets tend to spray out. (b) Gaseous jets can have much larger effective flow field than liquid jet even with smaller diameter nozzles.

dimension and the measured effective field, the spray angle of the gaseous nitrogen jet, θ , can be defined as

$$\theta = 2 \times \arctan \left(\frac{r_{\text{effective field}} - r_{\text{nozzle}}}{d_{\text{separation}}} \right) \quad (4)$$

where $r_{\text{effective field}}$ is the radius of effective flow field, r_{nozzle} the radius of the microfabricated nozzle, and $d_{\text{separation}}$ is the separation distance between the cantilever and the nozzle. For the tested pressure range from 6.8 to 10.6 MPa, the radius of effective flow field measured about 25 μm and separation distance was 27 μm . We conclude that the 1 μm diameter nozzle has a spray angle of about 84° for gaseous nitrogen jets.

Fig. 11 also shows the linear relationship between the cantilever maximum deflection and the driving pressure using gaseous nitrogen jets from the 1 μm diameter nozzle. Once the driving pressure is fixed, the cantilever maximum deflection can be estimated. Local thrust and velocity estimations for gaseous jets are not possible since the interaction between the cantilever and gaseous jets is more complicated because the gaseous jet sprays out and impinges on the cantilever with a finite angle other than 90°. If the piezoresistive cantilever approaches the nozzle exit within sub-micrometer proximity, the effective field of gaseous jets becomes small such that the thrust and velocity can be characterized as local flow properties.

4.2. Heated cantilever sensor

Heated cantilevers can detect changes in power dissipation and cooling capacity of micro/nanojets by heat transfer since heated cantilevers are very sensitive to small thermal agitation. The experiments above were repeated using a heated cantilever which has an integrated micro-heater near its free end to investigate the cooling capacity of the liquid and gaseous microjets and thermal transport between the cantilever heater and the impinging jet environment.

The heater region of the cantilever was aligned to and impinged by a liquid butane jet from a 10 μm diameter nozzle. Fig. 13 shows that the resistance of the heated cantilever changes with the dissipated power in the cantilever with and without jet impingement. Without jet impingement, the results show typical nonlinear electrical properties of the heated cantilever [40]. When the liquid butane jet impinges upon the cantilever heater region, the cantilever can dissipate more power without significant temperature rise. Fig. 13 also exhibits discontinuities representing local vaporization of a liquid butane droplet and each discontinuity is associated with a critical power. At each critical power, the cantilever electrical resistance and corresponding cantilever heater temperature increase all of a sudden and that critical power increases as the jet velocity increases.

A liquid butane droplet is observed around the heated cantilever legs at lower power than the critical power; however, the droplet vaporizes and disappears at higher power as shown in Fig. 14. Fig. 14(a) shows the heated cantilever and liquid butane jet from the 10 μm diameter nozzle before the cantilever heater is submerged in the butane jet. Fig. 14(b–d) shows that the liquid butane jet impinges on the heating element near the free end of

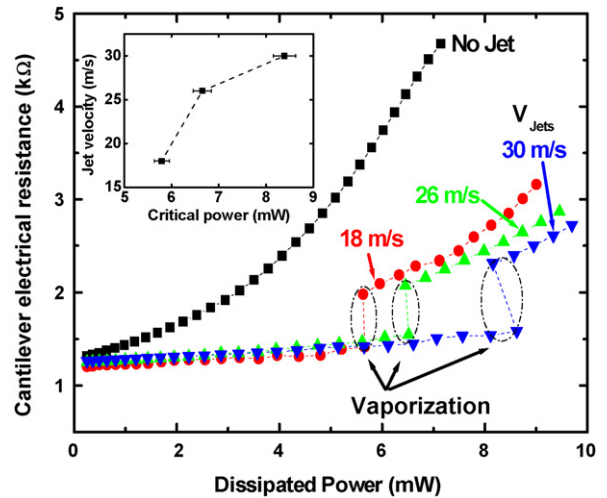


Fig. 13. Resistance of a heated cantilever as a function of dissipated power with and without additional cooling by liquid microjets. Without jet impingement, the results show typical nonlinear electrical properties of the heated cantilever. With jet impingement, the cantilever can dissipate more power without significant temperature rise. There are discontinuities representing local vaporization of liquid butane droplet and each discontinuity is associated with a critical power. The inset shows the critical power increases as the jet velocity increases.

the cantilever at different cantilever powers where the measured jet velocity is 18 m/s. When the cantilever power is 5.5 mW or less, a liquid butane droplet is observed around the heated cantilever legs. As power increases, the size of the droplet tends to decrease. The butane droplet vaporizes completely when the cantilever power is increased beyond 6.0 mW. Before the liquid droplet vaporizes, the cantilever is almost fully surrounded by the cold liquid jet environment and resistance versus power (R versus P) plots are independent of the jet velocity. Once the droplet vaporizes completely, the heated cantilever can dissipate more power at same electrical resistance as the jet velocity increases as shown in Fig. 13. Measured power when the vaporization occurs definitely depends on the droplet size. However, it is not possible to separate the measured power into dissipation due to vaporization and dissipation due to impinging jet near the cantilever free end since we only measured total power dissipation.

Micromachined hot-wire flow sensors [7] have been developed by several research groups to provide high spatial resolution, better uniformity, fast time response, and mass productivity. They have a thin wire element which acts as both Joule heater and temperature sensor and two parallel prongs which support the wire element and act as electrical leads. In steady state operation, the power generated by Joule heating is balanced by convection to the external flow and conduction through the support prongs. They are designed to minimize conduction heat loss through the support prongs in order to enhance sensitivity. The thermal measurement using the heated cantilever mimics HWA. Heated cantilevers can be operated with constant driving current or fixed heater temperature using appropriate feedback loops such that a constant temperature or a constant current anemometer can be constructed based on the heated cantilever. The heated cantilever herein has a resistive heater area sized

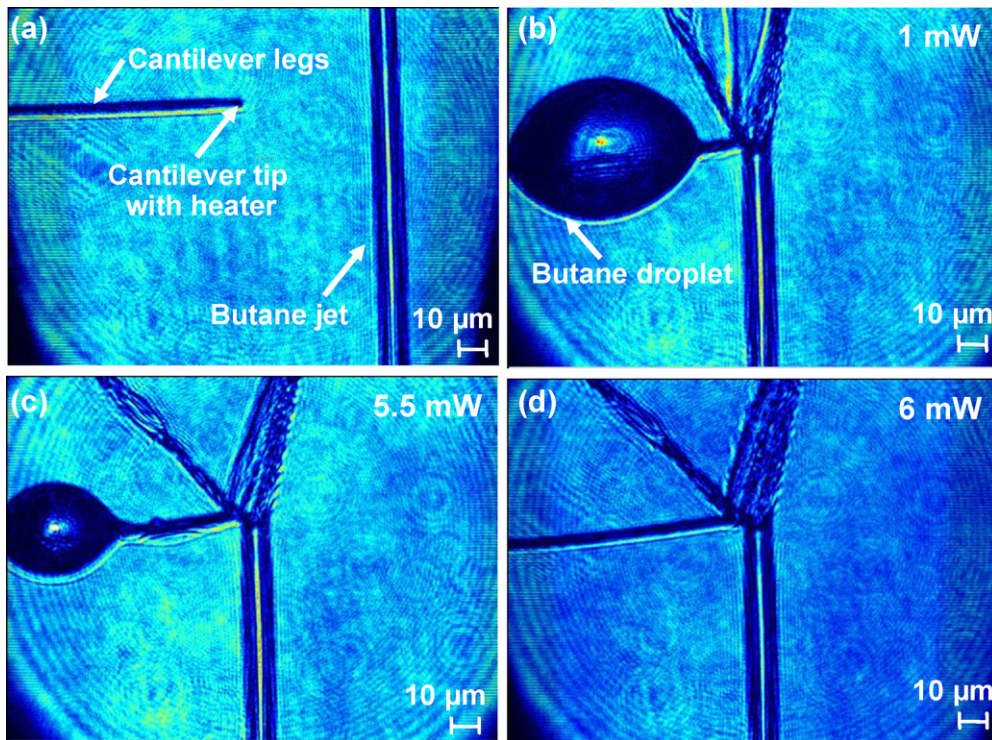


Fig. 14. (a) The heated cantilever and liquid butane jets from a $10\ \mu\text{m}$ diameter nozzle before the heating element is submerged into the butane jets. The liquid butane jets impinge on the heating element near free end of the cantilever at different cantilever powers where the measured jet velocity is 18 m/s. Cantilever powers are: (b) 1 mW, (c) 5.5 mW, and (d) 6 mW, respectively.

$5\ \mu\text{m} \times 10\ \mu\text{m}$ and the heater region was directly exposed to jet impingement. Therefore, gaseous jets which spray out or liquid jets from a nozzle larger than $10\ \mu\text{m}$ are preferred to fully immerse the heater area in the jet environment. To measure liquid jets from much smaller nozzles, the heater size should be scaled down. In contrast to micromachined hot-wire sensors, a significant amount of heat conducts through the cantilever legs and it depends upon the external environment. Therefore, a heat transfer simulation including relevant heat transfer mechanisms is required to estimate cooling capacity or heat transfer coefficients of microjets.

Using the thermal resistance network employed in previously published analyses of heat transfer in the heated cantilever [15,41,42], a one-dimensional finite difference heat transfer simulation was performed to estimate the thermal conductance – cooling capacity – via the microjets. With the cantilever heater temperature maintained at $150\ ^\circ\text{C}$, the thermal conductances between liquid butane jets and the cantilever heating element were 0.0197, 0.0231, and 0.0275 mW/K when the jets velocities were 18, 26, and 30 m/s, respectively. These numbers are comparable to heat transfer accompanied by phase change [43].

Heated cantilevers were also tested with gaseous nitrogen jets from the $10\ \mu\text{m}$ diameter nozzle. Fig. 15 shows the cantilever electrical resistance as a function of the dissipated power in the cantilever at various driving pressures where the heated cantilever is located $700\ \mu\text{m}$ above the nozzle exit. First, the electrical responses of the heated cantilever remain unchanged

as long as the driving pressure is less than 1.36 MPa. As the pressure increases, the R versus P curves are shifted to higher powers such that the cantilever can dissipate more power at fixed cantilever heater temperature. At pressure higher than 8.16 MPa, the flow velocity of the nitrogen jet becomes saturated and no more changes in the electrical response will be expected beyond this pressure. Since the heated cantilever is strongly sensitive to

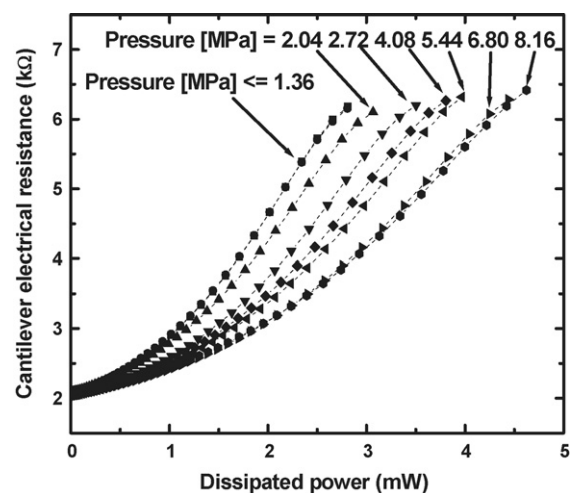


Fig. 15. Cantilever electrical resistance as a function of dissipated power in the cantilever at various gaseous nitrogen jet driving pressures where a $10\ \mu\text{m}$ diameter nozzle is used with $700\ \mu\text{m}$ separation between the cantilever and the nozzle.

any change which affects the heat transfer, it can be inferred that the momentum of the nitrogen jet becomes negligible at pressures less than 1.36 MPa with a separation distance of 700 μm between the cantilever and the nozzle. The shifted R versus P curves in the intermediate pressure ranges indicate the enhanced cooling capacity of nitrogen jets.

The gaseous nitrogen jet sprays out such that the effective flow field and momentum of the gaseous jet strongly depend on the separation distance between the cantilever and the nozzle. Therefore, the separation distance is a very important parameter required to explore for gaseous micro/nanojets.

5. Conclusions

Liquid butane and gaseous nitrogen jets generated from 1 to 12 μm diameter nozzles have been characterized with piezoresistive and heated microcantilever sensors. Our results show that the piezoresistive cantilevers measure jet thrusts ranging from 30 to 75 μN and estimate jet velocities of 40–60 m/s during liquid butane microjets impingement from a 6 μm diameter nozzle. Estimated jet velocities agree to the shadowgraphy results within 12.5% without introducing any correction factor. More accurate velocity measurement can be made with nozzles having sub-micrometer diameter without any correction factor since the momentum transfer correction factor will approach unity as the nozzle size gets much smaller. The piezoresistive cantilever sensors can also investigate the effective flow field, estimate spray angle of the gaseous jet, and inspect nozzle clogness.

With the heated cantilever, local vaporization of butane droplets and the localized cooling capability of the liquid microjets were examined. Finite difference heat transfer simulations showed the cooling capacity of the liquid butane microjet was in the order of 10^{-5} W/K for single phase cooling. There was a critical power indicating vaporization of the liquid butane droplet and the critical power increased with jet velocity. The heated cantilever could also detect small changes in the jet velocity and flow rate of gaseous jets.

Our results demonstrate novel microcantilever-based metrology for investigating both liquid and gaseous micro/nanoscale jets.

Acknowledgment

The work has been supported by the National Science Foundation under Grant # 0304009.

References

- [1] D.V. Palanker, D.A. Fletcher, J. Miller, P. Huie, M. Marmor, M.S. Blumenkranz, Pulsed liquid microjet for intravascular injection, *Proc. SPIE Opt. Technol.* 4611 (2002) 72–75.
- [2] D.A. Fletcher, D.V. Palanker, Pulsed liquid microjet for microsurgery, *Appl. Phys. Lett.* 78 (2001) 1933–1935.
- [3] D.J. Hayes, D.B. Wallace, W.R. Cox, Microjet printing of solder and polymers for multi-chip modules and chip-scale packages, *Proc. SPIE – Int. Conf. High Density Packaging and MCMs* 3830 (1999) 242–247.
- [4] E.N. Wang, L. Zhang, L. Jiang, J.-M. Koo, J.G. Maveety, E.A. Sanchez, K.E. Goodson, T.W. Kenny, Micromachined jets for liquid impingement cooling of VLSI chips, *J. Microelectromech. Syst.* 13 (2004) 833–842.
- [5] D.S. Kercher, J. Lee, O. Brand, M.G. Allen, A. Glezer, Microjet cooling devices for thermal management of electronics, *IEEE Trans. Comp. Pack. Tech.* 26 (2003) 359–366.
- [6] O.D. Sibailly, F.R. Wagner, L. Mayor, B. Richerzhagen, High precision laser processing of sensitive materials by microjet, in: *Fourth International Symposium on Laser Precision Microfabrication*, 2003, pp. 501–504.
- [7] J. Chen, C. Liu, Development and characterization of surface micromachined, out-of-plane hot-wire anemometer, *J. Microelectromech. Syst.* 12 (2003) 979–988.
- [8] G. Binnig, C.F. Quate, C. Gerber, Atomic force microscope, *Phys. Rev. Lett.* 56 (1986) 930–933.
- [9] G. Meyer, N.M. Amer, Novel optical approach to atomic force microscopy, *Appl. Phys. Lett.* 53 (1988) 1045–1047.
- [10] S. Alexander, L. Hellemans, O. Marti, J. Schneir, V. Elings, An atomic-resolution atomic-force microscope implemented using an optical lever, *J. Appl. Phys.* 65 (1989) 164–167.
- [11] M. Tortonesi, R. Barrett, C. Quate, Atomic resolution with an atomic force microscope using piezoresistive detection, *Appl. Phys. Lett.* 62 (1993) 834–836.
- [12] B.W. Chui, T.W. Kenny, H.J. Mamin, B.D. Terris, D. Rugar, Independent detection of vertical and lateral forces with a sidewall-implanted dual-axis piezoresistive cantilever, *Appl. Phys. Lett.* 72 (1998) 1388–1390.
- [13] M. Napoli, B. Bamieh, K. Turner, A capacitive microcantilever: modelling, validation, and estimation using current measurements, *J. Dyn. Syst., Meas., Contr.* 126 (2004) 319–326.
- [14] G. Binnig, M. Despont, U. Drechsler, W. Häberle, M. Lutwyche, P. Vettiger, H.J. Mamin, B.W. Chui, T.W. Kenny, Ultrahigh-density atomic force microscopy data storage with erase capability, *Appl. Phys. Lett.* 76 (1999) 1329–1331.
- [15] W.P. King, T.W. Kenny, K.E. Goodson, G.L.W. Cross, M. Despont, U. Durig, H. Rothuizen, G. Binnig, P. Vettiger, Atomic force microscope cantilevers for combined thermomechanical data writing and reading, *Appl. Phys. Lett.* 78 (2001) 1300–1302.
- [16] J. Fricke, E. Obermeier, Cantilever beam accelerometer based on surface micromachining technology, *J. Micromech. Microeng.* 3 (1993) 190–192.
- [17] T. Thundat, G.Y. Chen, R.J. Warmack, D.P. Allison, E.A. Wachter, Vapor detection using resonating microcantilevers, *Anal. Chem.* 67 (1995) 519–521.
- [18] L.A. Pinnaduwaage, A. Gehl, D.L. Hedden, G. Muralidharan, T. Thundat, R.T. Lareau, T. Sulchek, L. Manning, B. Rogers, M. Jones, J.D. Adams, A microsensor for trinitrotoluene vapour, *Nature* 425 (2003) 474.
- [19] M. Su, S. Li, V.P. Dravid, Microcantilever resonance-based DNA detection with nanoparticle probes, *Appl. Phys. Lett.* 82 (2003) 3562–3564.
- [20] D. Lange, C. Hagleitner, A. Hierlemann, O. Brand, H. Baltes, Complementary metal oxide semiconductor cantilever arrays on a single chip: mass-sensitive detection of volatile organic compounds, *Anal. Chem.* 74 (2002) 3084–3095.
- [21] H.-C. Lee, J.-H. Park, J.-Y. Park, H.-J. Nam, J.-U. Bu, Design, fabrication and RF performances of two different types of piezoelectrically actuated ohmic MEMS switches, *J. Micromech. Microeng.* 15 (2005) 2098–2104.
- [22] E.O. Sunden, T.L. Wright, J. Lee, S.A. Graham, W.P. King, Room temperature chemical vapor deposition and mass detection on a heated atomic force microscope cantilever, *Appl. Phys. Lett.* 88 (2006) 033107.
- [23] P.E. Sheehan, L.J. Whitman, W.P. King, B.A. Nelson, Nanoscale deposition of solid inks via thermal dip pen nanolithography, *Appl. Phys. Lett.* 85 (2004) 1589–1591.
- [24] B.A. Nelson, W.P. King, A. Laracuente, P.E. Sheehan, L.J. Whitman, Direct deposition of continuous metal nanostructures by thermal dip-pen nanolithography, *Appl. Phys. Lett.* 88 (2006) 033104.
- [25] T. Nishimoto, S. Shoji, M. Esashi, Buried piezoresistive sensors by means of Mev ion implantation, *Sens. Actuators, A* 43 (1994) 249–253.
- [26] V. Gass, B.H. Van der Schoot, N.F. De Rooij, Nanofluid handling by micro-flow sensor based on drag force measurement, in: *IEEE Proceedings of MEMS, NY, USA, 1993*, pp. 162–172.

- [27] Y. Su, A.G.R. Evans, A. Brunnschweiler, G. Ensell, Characterization of a highly sensitive ultra-thin piezoresistive silicon cantilever probe and its application in gas flow velocity sensing, *J. Micromech. Microeng.* 12 (2002) 780–785.
- [28] J.E. Sader, Frequency response of cantilever beams immersed in viscous fluids with applications to the atomic force microscopy, *J. Appl. Phys.* 84 (1998) 64–76.
- [29] P.I. Oden, G.Y. Chen, R.A. Steele, R.J. Warmack, T. Thundat, Viscous drag measurements utilizing microfabricated cantilevers, *Appl. Phys. Lett.* 68 (1996) 3814–3816.
- [30] S. Barth, H. Koch, A. Kittel, J. Peinke, J. Burgold, H. Wurmus, Laser-cantilever anemometer: a new high-resolution sensor for air and liquid flows, *Rev. Sci. Instrum.* 76 (2005) 075110.
- [31] B.W. Chui, T.D. Stowe, Y.S. Ju, K.E. Goodson, T.W. Kenny, H.J. Mamin, B.D. Terris, R.P. Ried, Low-stiffness silicon cantilever with integrated heaters and piezoresistive sensors for high-density data storage, *J. Microelectromech. Syst.* 7 (1998) 69–78.
- [32] P. Vettiger, G. Cross, M. Despont, U. Drechsler, U. Duerig, B. Gotsmann, W. Haberle, M. Lantz, H. Rothuizen, R. Stutz, G. Binnig, The “Millipede”-nanotechnology entering data storage, *IEEE Trans. Nanotechnol.* 1 (2002) 39–55.
- [33] J. Lee, K. Naeli, H. Hunter, J. Berg, T.L. Wright, C. Courcimault, N. Naik, M.G. Allen, O. Brand, A. Glezer, W.P. King, Micro-cantilever based metrology tool for flow characterization of liquid and gaseous micro/nanojets, in: Proceedings of ASME IMECE, FL, USA, 2005.
- [34] N. Naik, C. Courcimault, J. Berg, H. Hunter, J. Lee, K. Naeli, T. Wright, M.G. Allen, O. Brand, A. Glezer, W.P. King, Fabrication and characterization of liquid and gaseous micro- and nanojets, in: Proceedings of ASME IMECE, FL, USA, 2005.
- [35] T.L. Wright, Design and fabrication of heated atomic force microscope cantilevers, M.S. Thesis, Woodruff School of Mechanical Engineering, Georgia Institute of Technology, Atlanta, GA, 2005.
- [36] T.S. Ravi, R.B. Marcus, D. Liu, Oxidation sharpening of silicon tips, *J. Vac. Sci. Technol.*, B 9 (1991) 2733–2737.
- [37] J. Lee, T.L. Wright, M.R. Abel, E.O. Sunden, S. Graham, W.P. King, Thermal conduction from microcantilever heaters in partial vacuum, *Appl. Phys. Lett.*, submitted for publication.
- [38] S.H. Crandall, N.C. Dahl, T.J. Lardner, *An Introduction to the Mechanics of Solids*, second ed., McGraw-Hill, New York, 1978.
- [39] B.R. Munson, D.F. Young, T.H. Okiishi, *Fundamentals of Fluid Mechanics*, fourth ed., Wiley, 2002.
- [40] M. Despont, J. Brugger, U. Drechsler, U. Durig, W. Haberle, M. Lutwyche, H. Rothuizen, R. Stutz, R. Widmer, G. Binnig, H. Rohrer, P. Vettiger, VLSI-NEMS chip for parallel AFM data storage, *Sens. Actuators, A* 80 (2000) 100–107.
- [41] W.P. King, T.W. Kenny, K.E. Goodson, G.L.W. Cross, M. Despont, U.T. Durig, H. Rothuizen, G. Binnig, P. Vettiger, Design of atomic force microscope cantilevers for combined thermomechanical writing and thermal reading in array operation, *J. Microelectromech. Syst.* 11 (2002) 765–774.
- [42] W.P. King, Design analysis of heated atomic force microscope cantilevers for nanotopography measurements, *J. Micromech. Microeng.* 15 (2005) 2441–2448.
- [43] F.P. Incropera, D.P. DeWitt, *Fundamentals of Heat and Mass Transfer*, fourth ed., Wiley, New York, 2002.

Biographies

Jungchul Lee received the BS and MS degrees in mechanical engineering from Seoul National University, Seoul, Korea, in 2001 and 2003, respectively. He is currently working toward the PhD degree at the Georgia Institute of Technology (Georgia Tech). He is developing micromachined thermal sensors and actuators and investigating thermal transport in micro/nanoscale devices.

Kianoush Naeli received the BS degree in electrical engineering from Sharif University of Technology, in 1999 and the MS degree in electronics from the University of Tehran, Iran, in 2001. Currently he is a doctoral candidate in the

Department of Electrical and Computer Engineering at Georgia Tech, where his research is focused on cantilever-based sensors.

Hanif Hunter received the BS in mechanical engineering from Georgia Tech in 2002. He is currently working toward a PhD at Georgia Tech. He is studying and characterizing micro- and nanoscale jets.

John Berg received the BS in mechanical engineering from Johns Hopkins University, Baltimore, MD, in 2003. He worked toward his PhD in mechanical engineering at Georgia Tech from 2003 to 2004 before leaving engineering to pursue a career in clinical psychology. He is currently working toward his PhD in clinical psychology at Emory University, Atlanta, GA.

Tanya Wright received the BS in mechanical engineering from Iowa State University, Ames, IA, in 1999. After 3 years with Motorola in their Automotive Electronics Division, she attended Georgia Tech where she received the MS in mechanical engineering in 2005. Her thesis focused on the fabrication of heated microcantilevers. She is currently working for Schlumberger in their product center in Paris, France.

Christophe Courcimault received the French equivalent of the BS degree in physics from INSA Toulouse and the French equivalent of the PhD degree in microelectronics and microengineering from the same school, in June 2005. His research, focusing on the development of microsystems for the fabrication of nanosystems, was carried out at Georgia Tech in Atlanta, GA. After graduating in June 2005, he joined the R&D department of a biomedical Atlanta-based company, CardioMEMS, Inc., where he develops implantable wireless pressure sensor.

Nisarga Naik received the BS in electrical Engineering from V.J.T.I., Mumbai University, India, in 2003. She is currently working toward her PhD at Georgia Tech. Her research involves fabrication and characterization of nanonozzles.

Mark Allen received the BA degree in chemistry, the BSE degree in chemical engineering, and the BSE degree in electrical engineering from the University of Pennsylvania, University Park, and the SM and PhD degrees from the Massachusetts Institute of Technology, Cambridge, in 1989. He joined the faculty of Georgia Tech, Atlanta, in 1989, where he currently holds the rank of professor and the J.M. Pettit Professorship in microelectronics. He is North American editor of the *Journal of Micromechanics and Microengineering*. His research interests are in the areas of micromachining and MEMS, in particular, the development and application of new fabrication technologies for micromachined devices and systems. Dr. Allen was General Co-Chair of the 1996 IEEE MEMS Conference.

Oliver Brand is an associate professor in the School of Electrical and Computer Engineering at the Georgia Institute of Technology. He received his diploma degree in physics from Technical University Karlsruhe, Germany, in 1990 and his PhD degree from ETH Zurich, Switzerland, in 1994. From 1995 to 1997, he worked as a postdoctoral fellow at Georgia Tech. From 1997 to 2002, he was a lecturer at ETH Zurich in Zurich, Switzerland, and Deputy Director of the Physical Electronics Laboratory (PEL). He is a co-editor of the Wiley/VCH book series *Advanced Micro and Nanosystems*, a member of the editorial board of *Sensors and Materials*, a member of the technical program and steering committees of the *IEEE Microelectromechanical Systems Conference*, and a co-recipient of the 2005 *IEEE Donald G. Fink Prize Paper Award*. His research interests are in the areas of CMOS-based microsystems, microsensors, MEMS fabrication technologies, and microsystem packaging.

Ari Glezer received the BS degree from Tel Aviv University, Israel, in 1974 and the MS and PhD degrees from the California Institute of Technology, Pasadena, in 1975 and 1981, respectively. Prior to joining the faculty of Georgia Tech, he was a faculty of the University of Arizona. He joined Georgia Tech in 1992, where he currently holds the rank of professor and the George W. Woodruff Chair in thermal systems. His research interests focus on the manipulation and control of shear flows in a broad range of applications, including reacting and nonreacting mixing processes, enhancement of the aerodynamic performance of airborne and underwater vehicles, small-scale combustion-driven power systems, jet thrust vectoring and noise reduction, fluidic-driven

heat transfer with an emphasis on electronic cooling, fluid atomization, and the development of novel fluidic actuator technologies including MEMS-based actuators.

William P. King received the BS degree in mechanical engineering from the University of Dayton in 1996 and the MS and PhD degrees in mechanical engineering from Stanford University, Stanford, CA, in 1998 and 2002, respectively.

Between 1999 and 2001, he spent 16 months in the Micro/NanoMechanics Group of the IBM Zurich Research Laboratory. In July 2002, he joined the faculty of the Woodruff School of Mechanical Engineering at Georgia Tech, Atlanta, as assistant professor. At Georgia Tech, his group works on thermal engineering of micro/nanomechanical devices, including thermomechanical data storage and nanoscale thermal processing. He is the winner of the NSF CAREER award (2003) and the DOE PECASE award (2005).